J. Hydrol. Hydromech., X, 2026, X, X–X
https://doi.org/
©2026 Felipe Eler et al., published by Slovak Academy of Sciences.
This work is licensed under the Creative Commons Attribution-NonCommercial-NoDerivatives 4.0 International Licence.

Journal of Hydrology and Hydromechanics

Uncertainty Assessment of Capillary Pressure Curves Measured Using Centrifuge Methods

Felipe Eler[1*], Martinus Th. van Genuchten[2,3], Paulo Couto[1]

[1] Department of Civil Engineering, Federal University of Rio de Janeiro, UFRJ, Rio de Janeiro, RJ, Brazil.
[2] Department of Nuclear Engineering, Federal University of Rio de Janeiro, UFRJ, Rio de Janeiro, RJ, Brazil.
[3] Department of Earth Sciences, Utrecht University, Utrecht, The Netherlands.
[*] Corresponding author. E-mail: felipe.eler@petroleo.ufrj.br

Abstract: The centrifuge technique (CT) is widely used across hydrology, petrophysics, and related disciplines to measure the water retention/capillary pressure curves, but standard data inversion methods lack uncertainty quantification and often cannot guarantee solution uniqueness. To address this, we present a novel Bayesian framework for inverting CT data that explicitly accounts for experimental uncertainties, provides confidence intervals, quantifies parameter covariance, and analyzes solution uniqueness. The framework was validated against synthetic first-drainage data (the desorption curve) across various curve shapes and noise levels, successfully recovering true capillary pressure curves. Application to experimental core samples of Indiana Limestone, Silurian Dolomite, and Upper Gray Berea yielded highly consistent results, demonstrating the framework's practical reliability. The approach also facilitates crucial non-uniqueness analyses, identifies parameter correlations, and offers strategies for improved solution stability. To promote transparency, reproducibility, and cross-disciplinary collaboration, the complete framework is publicly available as an open-source code on GitHub.

Keywords: Capillary Pressure Curve; Centrifuge Method; Uncertainty Quantification; Solution Uniqueness; Bayesian Inference.

1 INTRODUCTION

The capillary pressure or soil water retention curve is a fundamental constitutive relationship necessary for quantifying and simulating water storage and movement within the vadose zone (van Genuchten, 1980; Elango and Perkins, 2011; Rasoulzadeh et al., 2025). To align with standard conventions in soil science and hydrology, capillary pressure (P_c) is defined throughout this work strictly as a positive quantity (analogous to matric suction in unsaturated soils). Other applications use P_c curves in their modeling, such as carbon capture and storage (Di et al., 2025), contaminant transport in porous media (McCray and Falta, 1997), hydrocarbon reservoir management (Arab et al., 2021), and fluid infiltration into roads and building materials or other natural or engineered porous media (e.g., Aslannejad, 2017; Brunetti et al., 2016; Koubaa et al., 2018; Liu et al., 2025; Tavangarrad et al., 2019).

Since Hassler and Brunner (1945) introduced the centrifuge technique (CT) as an alternative to existing approaches for measuring the capillary pressure curve, centrifuge methods have evolved and become far more popular. The CT has been used to extend the measurement range of unsaturated hydraulic properties (Turturro et al., 2022), the first drainage curve (McPhee et al., 2015), the imbibition curve for core flooding support (Berg et al., 2021; Maas et al., 2019), and the USBM (U.S. Bureau of Mines) methodology to measure the wettability of petroleum reservoir rocks (e.g., Anderson, 1986). Similar CT approaches have been developed within the soil and hydrologic sciences (e.g., Conca and Wright, 1998; Nimmo and Mello, 1991; Šimůnek and Nimmo, 2005).

Centrifuge techniques require inverting the average to the inlet-face fluid saturations of a sample (Forbes, 1994). Eq. 1 provides the relationship between the average and local water saturation for the first drainage case:

$$\overline{S_w} = \frac{1}{(r_2 - r_1)} \int_{r_1}^{r_2} S_w(r)\,dr \tag{1}$$

where $\overline{S_w}$ is the average water saturation expressed as the fraction of the porous media volume occupied by the water, r_1 and r_2 are the distances, in centimeters, between the axis of rotation and the sample bases (i.e., the inner and outer radii), and $S_w(r)$ is the local saturation as a function of position r (see also Fig. 1). Several techniques have been proposed to solve Eq. 1. In a survey, Forbes (1997) used synthetic data (simulated experimental outputs generated using a synthetic capillary pressure curve derived from a known correlation) to evaluate the accuracy of available methods. He found that the second solution of Forbes (1994) and an inverse approach using cubic splines (Nordtvedt and Kolltveit, 1991) best represented this data.

While valuable, the approaches by Forbes (1994) and Nordtvedt and Kolltveit (1991) do not consider experimental uncertainties or estimate confidence intervals (CI). Additionally, using spline parameterization may raise concerns about the physical significance of the parameters. To improve the estimation of CT derived capillary pressure curves, we propose a new framework for centrifuge data inversion that accounts for experimental uncertainties, confidence intervals, and parameter covariance. The framework is based on Bayesian inference and can handle any parameterization in the form of $S_w = f(P_c)$, i.e., of water saturation as a function of P_c. In this work, we demonstrate the framework using the van Genuchten (1980) parameterization for both synthetic and experimental first drainage data.

2 MATERIAL AND METHODS

2.1 The inversion framework

The proposed framework is illustrated in Fig. 2. The model library contains capillary pressure correlations of Brooks and Corey (1964), van Genuchten (1980), and Chen (1992). The van Genuchten correlation was implemented for both unimodal and bimodal pore size distributions following the work of Durner (1994). Implementation of the framework requires information about the core properties, such as dimensions and pore volume, the fluid density, and the centrifuge inner and outer radii (r_1 and r_2). The framework data input parameters are the angular speeds and the associated displaced fluid productions. Additionally, the framework can receive prior parameter knowledge if available.

The computational implementation uses the emcee package (Foreman-Mackey et al., 2013), a Python-based ensemble sampler with multiple chains to sample several target probability distributions. Emcee offers flexible sampling options, ranging from the traditional Metropolis-Hastings algorithm (Hastings, 1970) to a more recent kernel-density-based algorithm (Farr et al., 2020).

The log-probability function in our framework considers the log-prior (if available) and the log-likelihood distributions given by:

$$\log P(\theta|data) = \log P(\theta) + \log L(\theta) \quad (2)$$

$$log\, L(\theta) = -\frac{1}{2}\sum_{i=1}^{N}\left(\frac{\overline{S_w}_{model,i} - \overline{S_w}_{data,i}}{\sigma}\right)^2 - \frac{N}{2} log(2\pi\sigma^2) \quad (3)$$

$$log\, P(\theta) = -\sum_{x\in\theta}\frac{1}{2}\left(\frac{x-\mu_x}{\sigma_x}\right)^2 \quad (4)$$

where θ is the parameter vector, $P(\theta|data)$ is the probability of θ given the available experimental data, $P(\theta)$ is the prior, $L(\theta)$ is the likelihood, σ is the estimated standard deviation of the experimental data, N is the number of observations, μ_x is the prior mean for the parameter x, and σ_x is the prior standard deviation for the parameter x.

The Python implementation is highly parallelizable and uses Numba's just-in-time class compiler for acceleration (http://numba.pydata.org), allowing sampling 50,000 states in under 2 minutes on an average laptop computer (10th Gen Core i7, 6-core, and 16 GB of RAM) running Ubuntu 24.04.

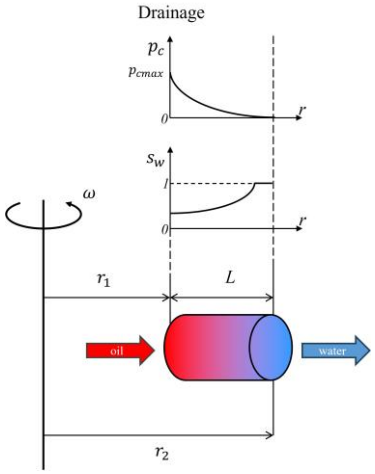


Fig. 1. Schematics of first drainage in the centrifuge: r_1 is the inner radius, r_2 is the outer radius, L is the core sample length, ω is the centrifugation speed, S_w is the water saturation and P_c is the capillary pressure. Adapted from Albuquerque et al. (2018).

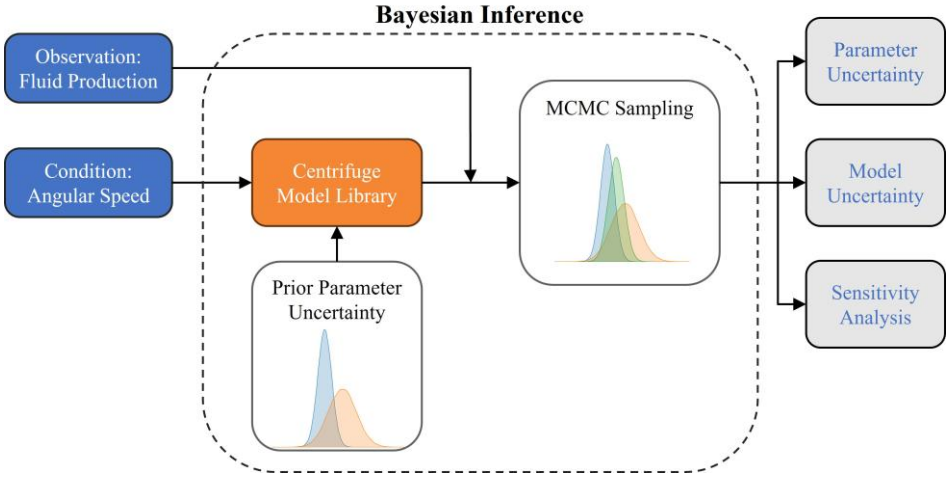


Fig. 2. Proposed framework for centrifuge data inversion. The model library needs experimental observations and conditions. Additionally, prior parameter knowledge can be informed. The framework provides parameter uncertainty, model uncertainty, and sensitivity analysis.

2.2 Synthetic First Drainage Data

The framework was first validated using synthetic data. Three curve shapes were used to generate synthetic first drainage laboratory data (Fig. 3). The curve shapes were generated using the capillary pressure curve of van Genuchten (1980) given by:

$$S_{wd} = \left[\frac{1}{1+(\alpha P_c)^n}\right]^m \tag{5}$$

$$S_{wd} = \frac{S_w - S_{wi}}{1 - S_{wi}} \tag{6}$$

where S_{wd} is the dimensionless water saturation (equivalent to soil water content, θ), α, m, and n are the correlation parameters, and S_{wi} is the irreducible or residual water saturation. The parameters of each shape in Fig. 1 are presented in Table 1.

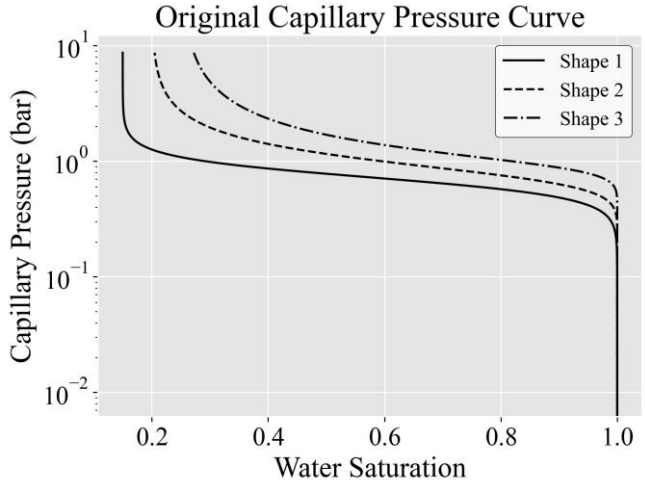


Fig. 3. Curve shapes used to generate synthetic centrifuge data and validate the Bayesian framework.

Table 1. Parameters used to generate curve shapes for the synthetic data.

Parameter	Shape 1	Shape 2	Shape 3
α (1/bar)	1.3797	1.6767	1.6809
m	1.0000	0.5251	0.2981
n	5.0000	3.6596	5.4705
P_d (bar)	0.0000	0.2068	0.3447
S_{wi}	0.15	0.20	0.25

To generate the average saturation data, Eq. 1 was written in terms of capillary pressures as suggested by Forbes (1994):

$$\overline{S_w}(P_{cmax}) = \frac{1+\sqrt{1-B}}{2}\int_0^1 \frac{S_w(xP_{cmax})}{\sqrt{1-Bx}}\,dx \tag{7}$$

$$B = 1 - \left(\frac{r_1}{r_2}\right)^2 \tag{8}$$

where P_{cmax} is the maximum capillary pressure on the core sample at centrifugation speed (ω), B is a geometric factor depending on the centrifuge outer radius (r_2) and the core sample length, (L), $r_1 = r_2 - L$, and x is an integration variable. The P_{cmax} was calculated using:

$$P_{cmax} = \frac{1}{2}\omega^2 \Delta\rho (r_2^2 - r_1^2) \tag{9}$$

in which $\Delta\rho$ is the density difference between the displaced and the displacing fluids.

Physical properties used to generate the synthetic data are based on a commercial ultracentrifuge by Core Lab Instruments and real rock and fluid properties (see Table 2). Random Gaussian noise was added to the synthetic data to avoid committing the inverse crime (Wirgin, 2004) and to evaluate the methodology's robustness, i.e., its sensitivity to experimental noise. An inverse crime occurs when the same (or close to the same) parameter values are used to synthesize as well as to invert data in an inverse problem. The noise levels assessed were 1.0, 2.5, and 5.0 saturation units (s.u.) These values represented the standard deviation of a Gaussian distribution given by

$$\overline{S_w}_{noisy} = \overline{S_w}_{truth} + \mathcal{N}(0, \sigma_{noise}) \tag{10}$$

where $\overline{S_w}_{noisy}$ is the average water saturation with added noise, $\overline{S_w}_{truth}$ is the true average water saturation, $\mathcal{N}$ is the normal distribution and σ_{noise} is the noise level.

2.3 Experimental First Drainage Data

After validating the framework with synthetic data, we analyzed the centrifuge experiments of three core outcrops purchased from Kocurek Industries. Petrophysical properties of the cores are presented in Table 3. The core samples were fully saturated with brine (200 g/l of NaCl), and isoparaffinic oil was used to displace the brine. The experiments were performed at ambient temperature using the ACES-300 automated centrifuge of Core Laboratories. The experimental conditions and results are presented in Tables 4 and 5, respectively.

Standard deviations of the experimental data were estimated using derivative propagation as recommended by the *Bureau International des Poids et Mesures* (BIPM et al., 2008):

$$y = f\left(x_1 \pm \sigma_{x_1}, x_2 \pm \sigma_{x_2}, x_3 \pm \sigma_{x_3}, \ldots\right) \tag{11}$$

$$\sigma_y = \sqrt{\left(\frac{\partial f}{\partial x_1}\sigma_{x_1}\right)^2 + \left(\frac{\partial f}{\partial x_2}\sigma_{x_2}\right)^2 + \left(\frac{\partial f}{\partial x_3}\sigma_{x_3}\right)^2 + \cdots} \tag{12}$$

where y is a variable of interest, determined by a function f, which takes as arguments the variables $x_{i=1,2,3,\ldots}$, σ_y is the standard deviation of the variable y, while σ_{x_i} are the standard deviations of the variables $x_{i=1,2,3,\ldots}$. The average standard deviations across the three experiments ranged from 3 to 4 s.u.; the results are presented in Fig. 4.

2.4 Optimization strategy

To ensure comprehensive sampling and assess the uncertainty of our estimated parameters, we employed a mixed ensemble sampling, with 50% of the steps utilizing the stretch move of Goodman and Weare (2010) and 50% utilizing a kernel-density-based move (Farr et al., 2020).

The ensemble size is ten times the number of estimated parameters, i.e., 50 walkers for the van Genuchten correlation (1980). The walkers were uniformly initialized across the entire range of each parameter (Table 5). This broad initialization strategy ensures that the Markov Chain Monte Carlo (MCMC) algorithm begins with a wide exploration of parameter space, minimizing bias from initial guesses and facilitating a thorough marginalization of the parameter distributions.

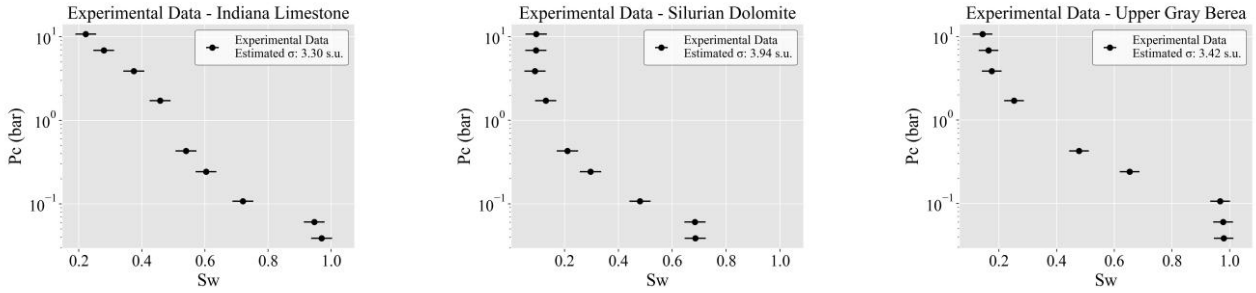


Fig.4. Experimental data and estimated noise level (σ) for the Indiana Limestone, Silurian Dolomite, and Upper Gray Berea core samples.

Table 2. Physical properties used to generate the synthetic experimental data.

Parameter	**Value**
Core Length (cm)	5.00
Core Diameter (cm)	3.81
Core Porosity (%)	20.0
Water Density (g/cm³)	1.141
Oil Density (g/cm³)	0.845
External Radius (cm)	9.13
Internal Radius (cm)	4.13
Angular Speeds (rpm)	300, 450, 600, 750, 1000, 1250, 1500, 1750, 2000, 2500, 3000, 3500, 4000, 4500, 5000, 5500, 6000, 6500, 7000, 7500, 8000, 8500, 9000

Table 3. Routine core analysis of the outcrops.

Core	**Lithology**	**Length L (cm)**	**Diameter D (cm)**	**Permeability k (mD)**	**Porosity ϕ (%)**
1	Indiana Limestone	5.02	3.77	84.3	19.1
2	Silurian Dolomite	5.00	3.79	242	15.9
3	Upper Gray Berea	4.94	3.74	170	19.1

Table 4. Experimental conditions for the drainage centrifugation experiments.

Brine Density (g/cm³)	1.1407
Oil Density (g/cm³)	0.8450
Initial Water Saturation (%)	100
Corelab's ACES-300 External Radius – r_2 (cm)	9.13

Table 5. Results of the drainage centrifugation experiments. The first line (0 rpm) shows the dead volume, which should be discounted from each reading.

Angular Speed (rpm)	**Water Production (cm³)**		
	IL	**SD**	**UGB**
0	8.00	8.00	8.00
600	8.32	10.82	8.21
750	8.57	10.83	8.23
1000	10.99	12.66	8.34
1500	12.24	14.31	11.58
2000	12.92	15.08	13.40
4000	13.80	15.80	15.73
6000	14.69	16.16	16.53
8000	15.71	16.13	16.64
10000	16.32	16.12	16.86

Table 6. Parameter marginalization ranges used for the van Genuchten model (1980).

Parameter	Minimum	Maximum
α (1/bar)	0.01	10
m	0	10
n	0	10
P_d (bar)	0	1
s_{wi}	0	1

To refine the quantification of uncertainties, we explored two distinct optimization strategies. The first approach involved a direct MCMC sampling run without any prior information. In this scenario, the MCMC solely relied on the likelihood function, which quantifies the agreement between the model predictions and the observed data.

The second strategy introduced a sequential optimization step to inform the MCMC sampling process. For this, we first performed a Least Squares (LS) optimization to obtain an initial set of optimal parameter values and their corresponding standard deviations. We used the Python package LMFIT (Newville et al., 2014) to perform the LS step. To mitigate potential initialization bias in the LS fit, we conducted 50 independent LS optimizations, each starting from a random initialization. From these 50 runs, we selected the one that yielded the best overall fit. These optimized results were used next to construct a prior distribution for the subsequent MCMC run, specifically as a Gaussian distribution.

A critical advantage of the invoked sequential approach is its adaptive nature. If the LS optimization yields a poor fit to the data, the calculated standard deviations for the parameters will be inherently high. The large standard deviation will translate directly into a weak or broad prior distribution for the MCMC, resulting in minimal influence on the sampling process. In such cases, the MCMC will still predominantly rely on the likelihood function of the data, maintaining the integrity of the posterior distribution even when the initial LS fit is suboptimal. This allows the MCMC to effectively explore parameter space without being unduly constrained by an inaccurate initial optimization.

Our framework offers significant flexibility as a user can readily incorporate prior information, if available, from other experiments (e.g., of the core sample itself or of a twin sample). This external information can directly replace the LS-derived prior with minimal modifications to the codebase, enabling seamless integration of diverse data sources into the MCMC sampling process.

2.5 Metrics for evaluating the results

To evaluate the quality of our results, we employed four distinct metrics. One concerns the Fréchet distances between the true and the estimated curves (Driemel et al., 2024), which quantify the overall similarity in curve shapes. This metric is available only for the synthetic data; the other three metrics can be applied to both synthetic and actual laboratory experiments. The second metric is the reduced chi-squared statistic, χ_v^2, which provides a measure of the goodness of fit between model predictions and the observed data relative to the expected variance. The reduced chi-squared is given by:

$$\chi_v^2 = \frac{\sum_{i=1}^{i=N}(Rsd_i)^2}{N-N_{params}} \tag{13}$$

where N is the number of available data points, N_{params} is the number of estimated parameters, and Rsd_i are the standardized residuals.

The third metric is the width of the CI at 95% (measured as the Fréchet distance between the 2.5% and the 97.5% percentiles), which reflects the degree of uncertainty in the curve estimate. As the fourth metric, we use the covariance between parameters, which evaluates the correlation among the estimated parameters and can indicate the uniqueness of the solution.

3 RESULTS AND DISCUSSION

3.1 Synthetic First Drainage Data

The framework was used to evaluate 18 problems: 3 curve shapes, 3 noise levels, and 2 optimization strategies. A summary of the metrics for all 18 cases is presented in Table 7. When comparing the optimization strategies, it becomes clear that incorporating prior information from the LS optimization leads to improvements across all metrics. Fig. 5 presents box plots for this comparison, while Fig. 6 illustrates the comparison by presenting the recovered curves for shape 1.

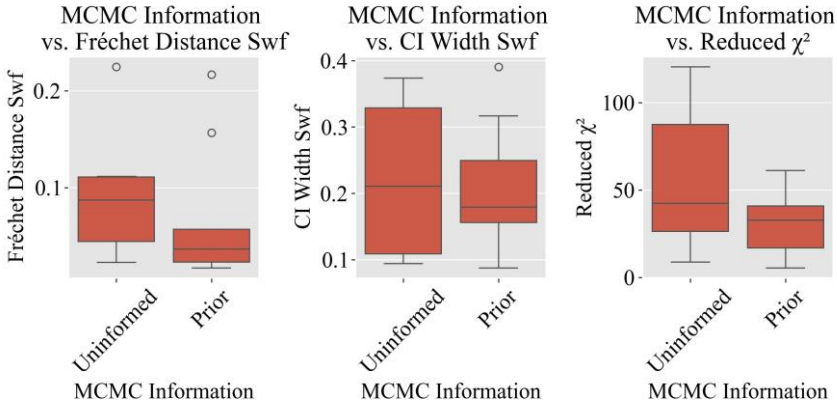


Fig. 5. Box plots comparing the optimization strategy's impact on the metrics used to evaluate the recovery of the ground-truth capillary pressure curve.

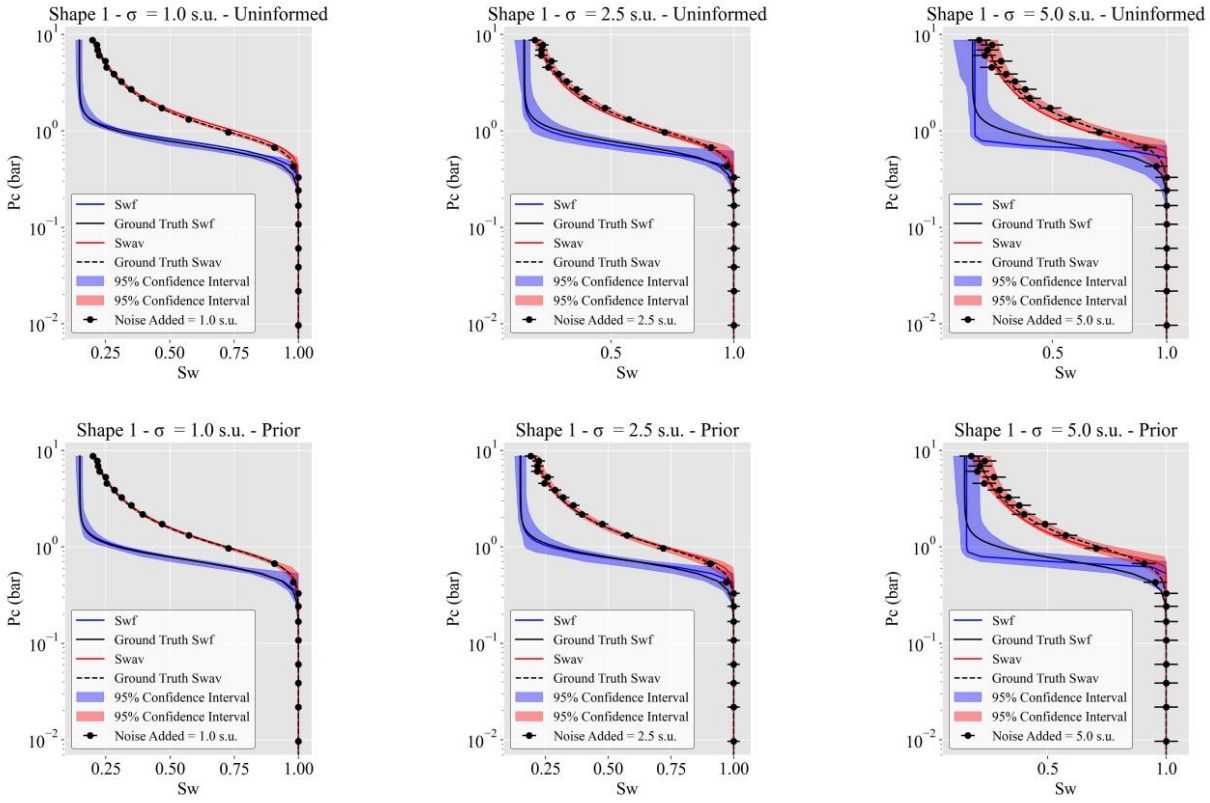


Fig. 6. Comparison of the optimization strategy for curve shape 1 and all noise levels. The estimation using prior information form LS optimization presented better results than the uninformed estimation.

Table 7. Summary of the results of the synthetic study. The Fréchet distance and the Confidence Interval (CI) width, and reduced chi-squared (χ_v^2) were calculated for the local saturation curves.

Curve	Noise Level	Optimization	Fréchet distance	CI Width	χ_v^2
Shape 1	1.0 s.u.	Uninformed	0.0661	0.1005	8.77
Shape 1	1.0 s.u.	Prior Given	0.0168	0.1290	16.82
Shape 1	2.5 s.u.	Uninformed	0.0871	0.2108	42.39
Shape 1	2.5 s.u.	Prior Given	0.0568	0.1790	39.61
Shape 1	5.0 s.u.	Uninformed	0.2247	0.3293	37.15
Shape 1	5.0 s.u.	Prior Given	0.2167	0.3167	28.92
Shape 2	1.0 s.u.	Uninformed	0.0225	0.1087	26.31
Shape 2	1.0 s.u.	Prior Given	0.0230	0.1559	14.86
Shape 2	2.5 s.u.	Uninformed	0.0298	0.2424	83.66
Shape 2	2.5 s.u.	Prior Given	0.0363	0.1788	40.74
Shape 2	5.0 s.u.	Uninformed	0.1109	0.3738	120.35
Shape 2	5.0 s.u.	Prior Given	0.1565	0.3905	61.11
Shape 3	1.0 s.u.	Uninformed	0.0443	0.0941	19.43
Shape 3	1.0 s.u.	Prior Given	0.0218	0.0875	5.34
Shape 3	2.5 s.u.	Uninformed	0.1114	0.1815	93.78
Shape 3	2.5 s.u.	Prior Given	0.0274	0.2024	32.69
Shape 3	5.0 s.u.	Uninformed	0.1040	0.3285	87.41
Shape 3	5.0 s.u.	Prior Given	0.0523	0.2493	46.23

The optimization strategy that uses prior information performed better for all metrics considered. Even with a low noise level of 1 s.u., which is unattainable in actual laboratory settings, prior information yielded better results than the uninformed strategy. Given the superior performance of incorporating prior information from the LS optimization, the effects of curve shape and noise level will be examined, while results from the uninformed strategy will be ignored.

Fig. 7 shows how the noise level affects the recovery of the capillary pressures. As expected, higher noise levels worsen all three metrics. Our framework produced consistent results across the entire range of noise levels evaluated, from the unrealistic low noise level of 1.0 s.u. to automated centrifuge noise levels of 2.5 to 5.0 s.u. Centrifuges that rely on visual level readings may have higher errors, in the order of 10 to 15 s.u., due to parallax errors or poor stabilization time (Fernø et al., 2007). In this range, even our robust approach would fail to recover the actual capillary pressure curve, as demonstrated in Fig. 8 for all curve shapes using an error of 12.5 s.u.

Our approach analyzed a reasonable range of first drainage shapes. The effect of curve shape on the recovery of the capillary pressure curves is presented in Fig. 9. The Fréchet distance indicates that shape 3 had the best result, followed by shapes 2 and 1. However, this may be a limitation of the correlation rather than of the framework itself. For example, shape 1 was recovered using Chen's second correlation (1992), yielding better results, as shown in Fig. 10.

Before moving from synthetic datasets to real experiments, we emphasize that the first metric is only applicable to synthetic datasets. We examined the relationship between the available metrics shown in Fig. 11 and found a good correlation between the CI and the Fréchet distances ($R^2 = 0.71$). The correlation between the CI and the χ_ν^2 is also reasonable ($R^2 = 0.62$). Given the good correlation, the second and third metrics should suffice for the experimental datasets evaluation.

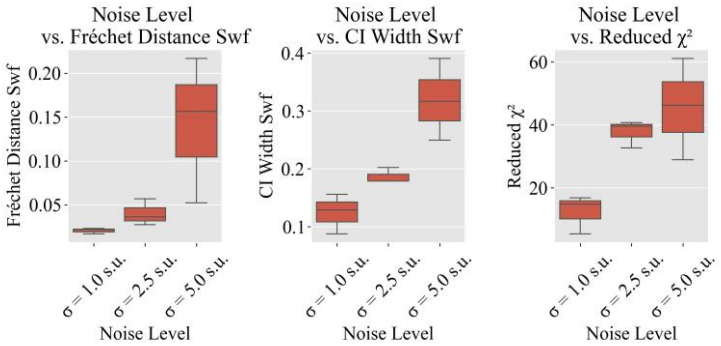


Fig. 7. Box plots comparing the noise level's impact on the metrics used to evaluate the recovery of the ground-truth capillary pressure curve (only data with prior information considered).

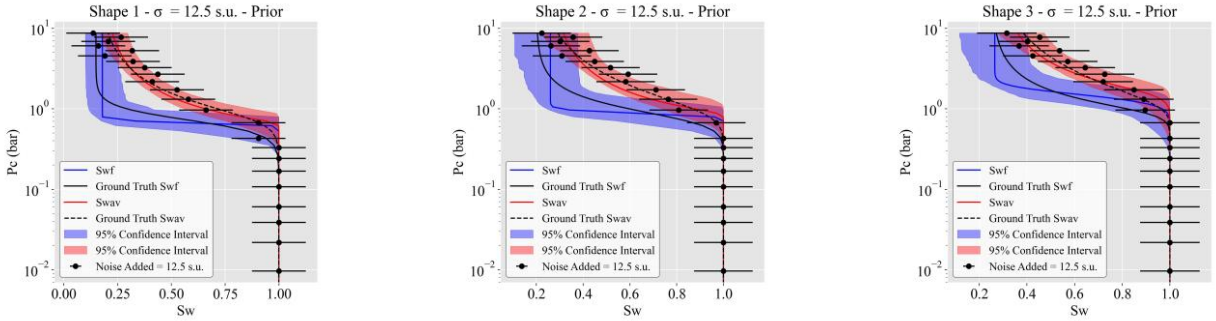


Fig. 8. Recovered curves for all three shapes using a noise level of 12.5 s.u. It is possible to observe poor agreement, even using priors.

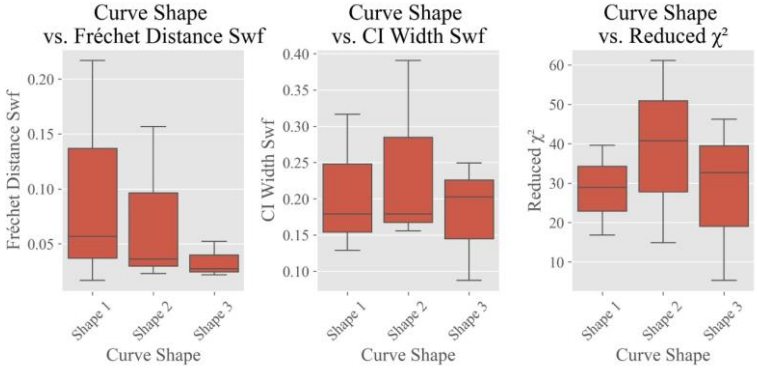


Fig. 9. Box plot comparing the curve shapes' impact on the metrics used to evaluate the recovery of the ground-truth capillary pressure curve (only data with prior information considered).

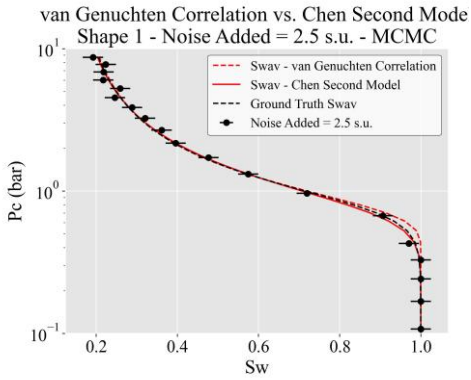


Fig. 10. Comparison between the van Genuchten and Chen parameterizations: Recovery of curve shape 2 with noise level of 2.5 s.u. The Van Genuchten correlation Fréchet distance was 0.0266, while the Chen correlation Fréchet distance was 0.0156.

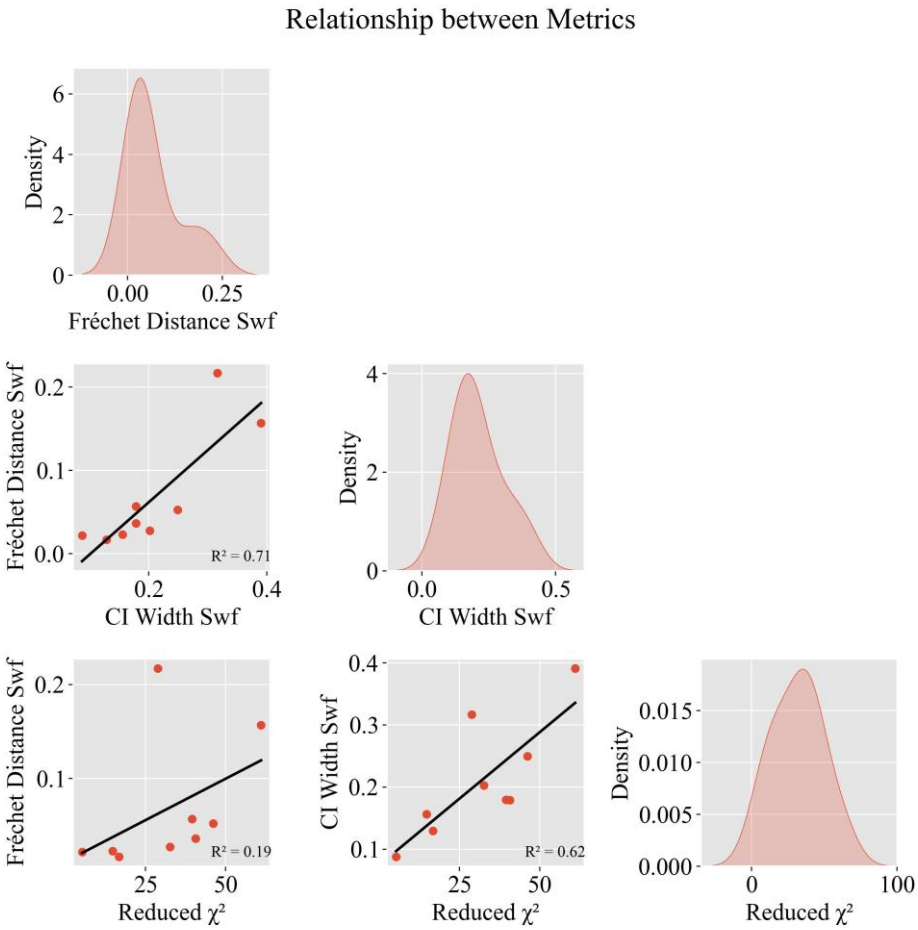


Fig. 11. Metric distributions and their correlations. Good correlations exist between the Fréchet distances and the Confidence Intervals (CI) width, and between the reduced chi-squared and the CI width. This supports the use of the CI width and the reduced chi-squared as proxy metrics for the Fréchet distances.

3.2 Experimental first drainage data

The validated workflow was used to recover the capillary pressure of three centrifuge experiments. Fig. 12 presents the recovered capillary pressure curves (P_c-S_w) for the Indiana Limestone, Silurian Dolomite, and Upper Gray Berea core samples, while Table 8 presents a summary of the metrics for the three experiments. Notice that the CI widths observed for all experimental samples are comparable to the best results achieved with the synthetic data. Given the strong correlation between the CI width and the Fréchet distance demonstrated previously (R^2 = 0.71) and the robustness of the framework, we assume that the P_c curves were consistently recovered.

Another feature of the framework is its ability to check for solution uniqueness and parameter correlations. Fig. 13 presents the posterior distributions of the parameters and a cross-plot of parameter pairs. We can observe α and m have wider distributions than the other parameters and are also the pair with the strongest correlation.

A customary practice is to fix one of the two parameters and let the other vary freely. The parameter α was set to 5.0, and the framework was executed again; the new results are presented in

Figs. 14 and 15. The excessive parameter correlation was eliminated, and all distributions became more normal-like. The cross-plots became rounder, eliminating the elliptical aspect. These results are strong indicators of improved solution uniqueness (Berg et al., 2021).

Table 8. Summary of the results from the experimental datasets. The Confidence Interval (CI) widths were calculated for the local saturation curves.

Core	Lithology	Estimated Noise Level	CI Width	χ_v^2
1	Indiana Limestone	3.30	0.1282	3.51
2	Silurian Dolomite	3.94	0.1995	3.10
3	Upper Gray Berea	3.42	0.1989	0.41

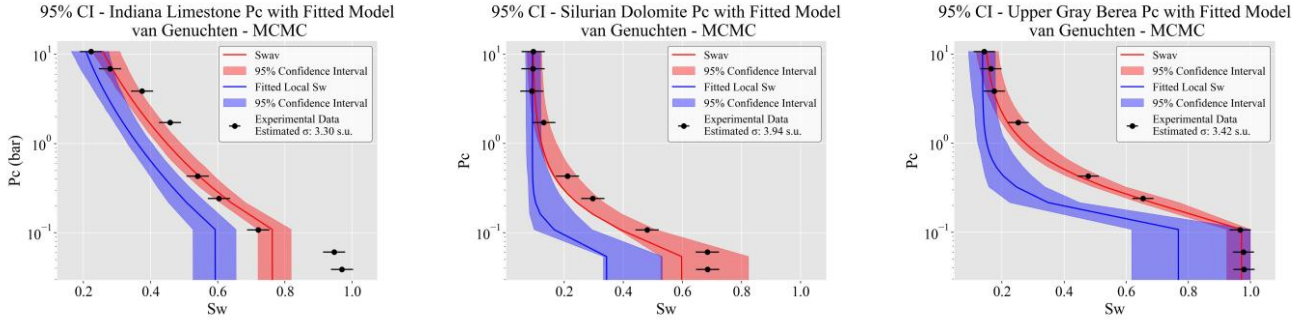


Fig. 12. Recovered capillary pressure for: a) Indiana Limestone, b) Silurian Dolomite, and c) Upper Gray Berea.

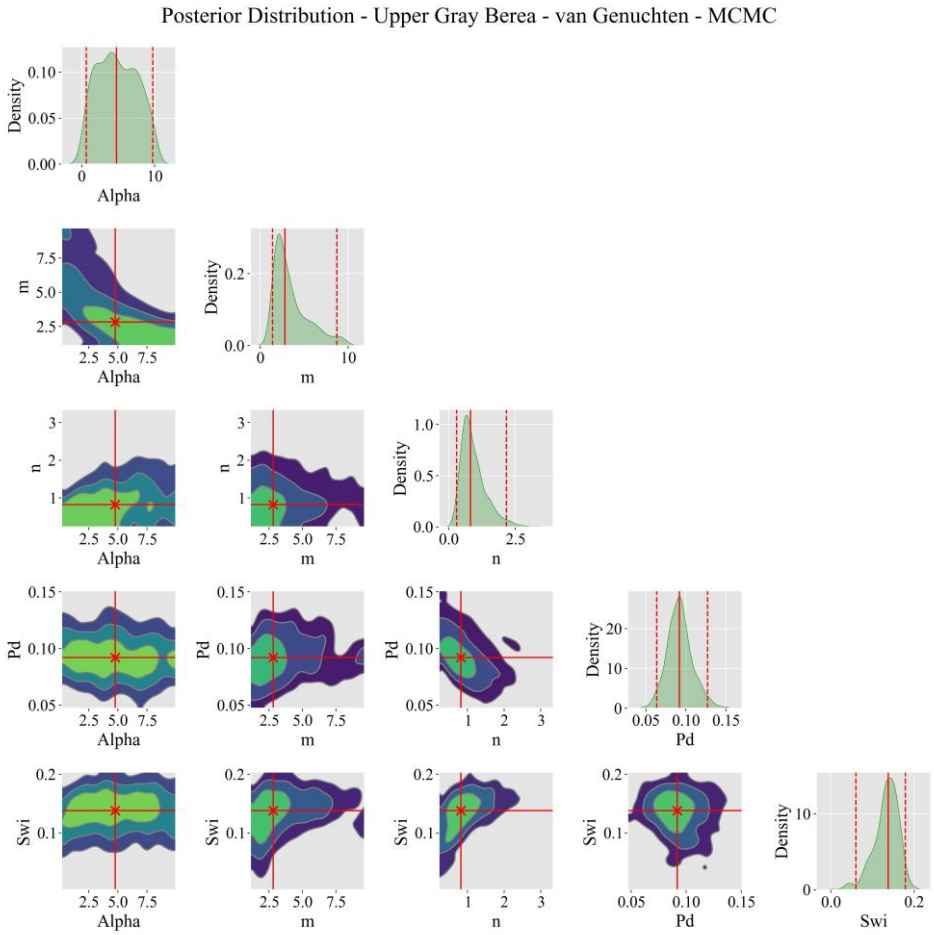


Fig. 13. Parameters' posterior distribution and cross-plot for the Upper Gray Berea. The solid red lines are the distribution median (percentile = 50%), and the dashed red lines delimit the 95% confidence interval for the parameter. The r2 score indicates parameter correlations.

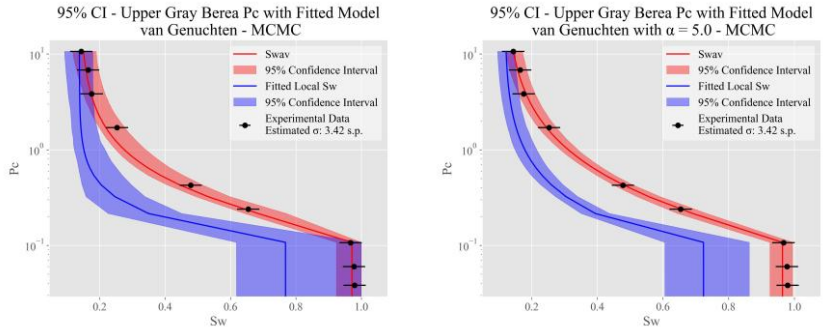


Fig. 14. Comparison of the recovered capillary pressure curves for the Upper Gray Berea experiment with and without fixing the parameter α at 5.0 bar -1. Reducing the number of parameters to be estimated reduced significantly the CI width.

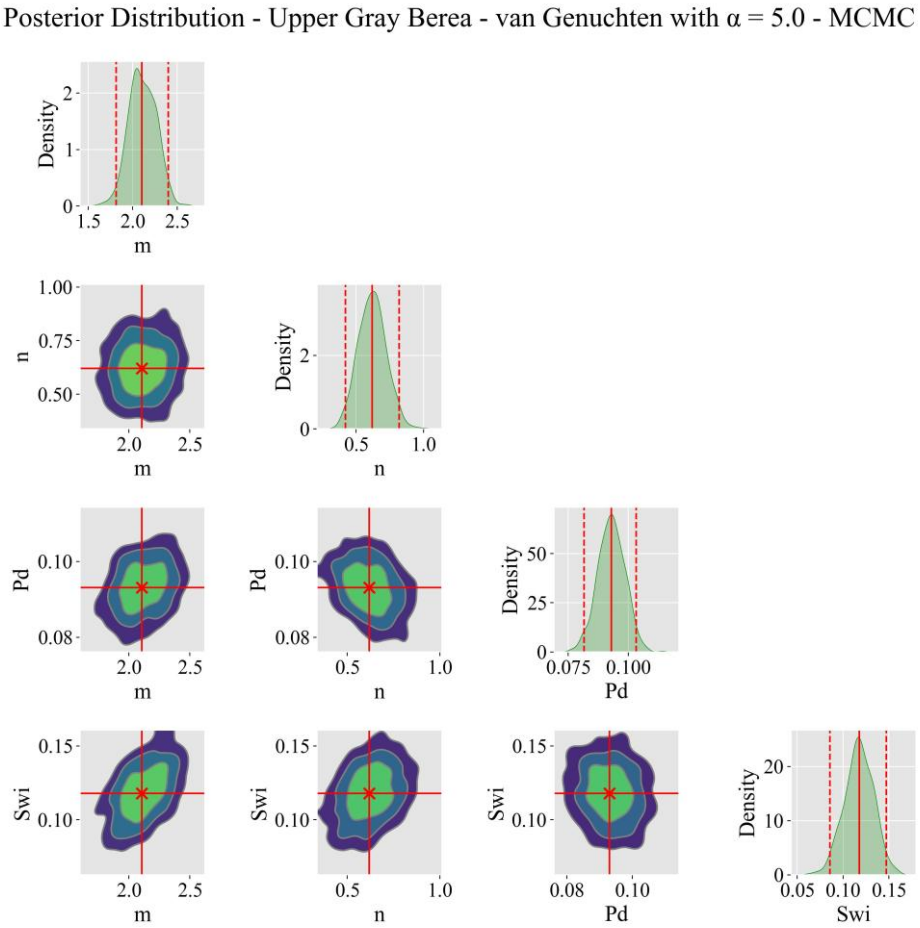


Fig. 15. Parameter posterior distributions and cross-plots for the Upper Gray Berea sample with parameter α fixed at 5.0 bar -1. The solid red lines are the distribution median (percentile = 50%), and the dashed red lines delimit the 95% confidence interval for the parameter. Reducing the number of parameters to be estimated turned the cross-plots rounder, eliminating the elliptical aspect. This is a strong indicator of improved solution uniqueness.

4 CONCLUSIONS

This study presents a novel and versatile framework for the inversion of centrifuge data into capillary pressure curves, specifically designed to account for experimental uncertainties, provide Confidence Intervals (CI), quantify parameter covariance, and analyze solution uniqueness. The framework was initially validated using synthetic first drainage data across various curve shapes and noise levels. Key findings from this validation are the reliability of the optimization strategy, the robustness of the framework for errors between 1.0 and 5.0 s.u., and the strong agreement observed between the Fréchet distance and the CI width metrics, with a notable correlation coefficient (R^2) of 0.71. This strong correlation provides a robust indicator that the CI width, which applies to both synthetic and real experimental data, can reliably serve as a proxy for the overall accuracy of the recovered capillary pressure curves.

After successful validation, the framework was applied to real experimental first drainage data obtained from three distinct core outcrops: Indiana Limestone, Silurian Dolomite, and Upper Gray

Berea. Application to these real-world scenarios demonstrated the framework's practical utility and effectiveness in recovering capillary pressure curves with significant reliability. The CI widths obtained from the experimental data were consistent with the best results achieved during the synthetic data validation, thereby further reinforcing the framework's capability to handle the inherent complexities and uncertainties typical of actual laboratory measurements and, hence, its promise for improving centrifuge measurements in the soil, hydrology, and petrophysics disciplines.

A critical aspect of the proposed framework is its capability to perform uniqueness analysis and assess parameter correlations. We demonstrated how to handle potential non-uniqueness issues, such as strong parameter correlations and wide posterior distributions. This in-depth analysis of parameter space and uncertainty propagation significantly advances over traditional methods by offering a more complete picture of the inversion results.

To foster transparency, reproducibility, and collaborative development within the scientific community, the entire framework, including all computational implementations, is publicly available as an open-source code on GitHub (https://github.com/felipeeler/centrifuge). This open-source release will significantly benefit the soil, hydrology, and petrophysics communities by providing a powerful and flexible tool for uncertainty quantification of capillary pressure curve experiments. The code has a step-by-step tutorial on how to use it.

Acknowledgment: This research was carried out in association with ongoing R&D project registered as ANP nº 23020-1, "Caracterização Experimental, Modelagem e Otimização de Processos de Injeção de Água Alternada Com Gás – WAG-EX Fase II" (UFRJ/Shell Brasil/ANP), sponsored by Shell Brasil Petróleo Ltda under the ANP R&D levy as "Compromisso de Investimentos com Pesquisa e Desenvolvimento".

REFERENCES

Albuquerque, M. R., Eler, F. M., Camargo, H. V. R., Compan, A. L. M., Cruz, D. A., Pedreira, C. E., 2018. Estimation of capillary pressure curves from centrifuge measurements using inverse methods. Rio Oil & Gas Conference, 19, 1–10. https://biblioteca.ibp.org.br/riooilegas/pt-BR/search/38799

Anderson, W. G., 1986. Wettability literature survey—Part 2: Wettability measurement. Journal of Petroleum Technology, 38(11), 1246–1262. https://doi.org/10.2118/13933-PA

Arab, D., Kantzas, A., Torsæter, O., Akarri, S., Bryant, S.L., 2021. A Crucial Role of the Applied Capillary Pressure in Drainage Displacement. SPE Journal 26, 2148–2166. https://doi.org/10.2118/200624-PA

Aslannejad, H., Hassanizadeh, S.M., Raoof, A., De Winter, D.A.M., Tomozeiu, N., Van Genuchten, M.Th., 2017. Characterizing the hydraulic properties of paper coating layer using FIB-SEM tomography and 3D pore-scale modeling. Chemical Engineering Science 160, 275–280. https://doi.org/10.1016/j.ces.2016.11.021

Berg, S., Unsal, E., Dijk, H., 2021. Non-uniqueness and uncertainty quantification of relative permeability measurements by inverse modelling. Computers and Geotechnics, 132, 103964. https://doi.org/10.1016/j.compgeo.2020.103964

BIPM, IEC, IFCC, ILAC, ISO, IUPAC, IUPAP, & OIML. (2008). Evaluation of measurement data—Guide to the expression of uncertainty in measurement. https://www.bipm.org/documents/20126/2071204/JCGM_100_2008_E.pdf/cb0ef43f-baa5-11cf-3f85-4dcd86f77bd6

Brooks, R. H., Corey, A. T., 1964. Hydraulic Properties of Porous Media and Their Relation to Drainage Design. Transactions of the ASAE, 7(1), 26–0028. https://doi.org/10.13031/2013.40684

Brunetti, G., Šimůnek, J., Piro, P., 2016. A comprehensive numerical analysis of the hydraulic behavior of a permeable pavement. Journal of Hydrology 540, 1146–1161. https://doi.org/10.1016/j.jhydrol.2016.07.030

Chen, Z., Liu, H., Yao, J., 1992. New capillary pressure models for parameter estimation to interpret centrifuge data. SPE Western Regional meeting, 221–228. https://doi.org/10.2118/24045-MS

Conca, J.L., Wright, J., 1998. The UFA method for rapid, direct measurements of unsaturated transport properties in soil, sediment, and rock. Australian Journal of Soil Research 36, 291–316. https://doi.org/10.1071/S96019

Di, C., Wei, Y., Wang, K., Deng, P., Chen, B., Shen, L., Chen, Z., 2025. The impact of pressurization-induced decrease of capillary pressure and residual saturation on geological carbon dioxide storage. Journal of Cleaner Production, 486, 144573. https://doi.org/10.1016/j.jclepro.2024.144573

Driemel, A., van der Hoog, I., Rotenberg, E., 2024. On the discrete Fréchet distance in a graph. Journal of Computational Geometry, 14(2). https://doi.org/10.20382/jocg.v14i2a9

Durner, W., 1994, Hydraulic conductivity estimation for soils with heterogeneous pore structure. Water Resources Research, 30(2), 211–223. https://doi.org/10.1029/93WR02676

Elango, L., Perkins, K. S., 2011. Hydraulic conductivity—Issues, determination, and applications. In Hydraulic Conductivity—Issues, Determination and Applications. IntechOpen. https://doi.org/10.5772/744

Farr, B., Farr, W., Rudd, D., Price-Whelan, A., Macleod, D., 2020. Kombine: Kernel-density-based parallel ensemble sampler. Astrophysics Source Code Library, ascl:2004.010.

Fernø, M.A., Treinen, R., Graue, A. 2007. Experimental Measurements of Capillary Pressure with the Centrifuge Technique – Emphasis on Equilibrium Time and Accuracy in Production. International Symposium of the Society of Core Analysts, Calgary, AB, Canada. https://jgmaas.com/SCA/2007/SCA2007_22.pdf

Forbes, P., 1994. Simple and accurate methods for converting centrifuge data into drainage and imbibition capillary pressure curves. The Log Analyst, 35(04). https://onepetro.org/petrophysics/article/170846/Simple-And-Accurate-Methods-For-Converting

Forbes, P., 1997. Centrifuge data analysis techniques: An SCA survey on the calculation of drainage capillary pressure curves from centrifuge measurements. International Symposium of the Society of Core Analysts, Calgary, AB, Canada. https://jgmaas.com/SCA/1997/SCA1997-14.pdf

Foreman-Mackey, D., Hogg, D. W., Lang, D., Goodman, J., 2013. emcee: The MCMC Hammer. Publications of the Astronomical Society of the Pacific, 125(925), 306–312. https://doi.org/10.1086/670067

Goodman, J., Weare, J., 2010. Ensemble samplers with affine invariance. Communications in Applied Mathematics and Computational Science, 5(1), 65–80. https://doi.org/10.2140/camcos.2010.5.65

Hassler, G. L., Brunner, E., 1945. Measurement of capillary pressures in small core samples. Transactions of the AIME, 160(01), 114–123. https://doi.org/10.2118/945114-G

Hastings, W. K., 1970. Monte Carlo sampling methods using Markov chains and their applications. Biometrika, 57(1), 97–109. https://doi.org/10.1093/biomet/57.1.97

Koubaa, Y., Jamei, M., Guiras, H., 2018. Hydro-mechanical Properties of Highly porous Limestone Rock used for Historic Monuments in North-East Tunisia. J Civil Environ Eng 08. https://doi.org/10.4172/2165-784X.1000310

Liu, S., Bian, X., Cui, Y., Chen, Y., 2025. Full-Scale Experimental Study on the Degradation of Pile-Supported Embankment due to Water Infiltration. J. Geotech. Geoenviron. Eng. 151, 04025129. https://doi.org/10.1061/JGGEFK.GTENG-13201

Maas, J. G., Springer, N., Hebing, A., 2019. Defining a sample heterogeneity cut-off value to obtain representative Special Core Analysis (SCAL) measurements. International Symposium of the Society of Core Analysts, Pau, France. https://jgmaas.com/SCA/2019/SCA2019-024.pdf

McCray, J.E., Falta, R.W., 1997. Numerical Simulation of Air Sparging for Remediation of NAPL Contamination. Groundwater 35, 99–110. https://doi.org/10.1111/j.1745-6584.1997.tb00065.x

McPhee, C., Reed, J., Zubizarreta, I., 2015. Core analysis: A best practice guide. Elsevier.

Newville, M., Stensitzki, T., Allen, D. B., Ingargiola, A., 2014. LMFIT: Non-linear least-square minimization and curve-fitting for Python (version 0.8.0) [Computer software]. Zenodo. https://doi.org/10.5281/zenodo.11813

Nimmo, J.R., Mello, K.A., 1991. Centrifugal techniques for measuring saturated hydraulic conductivity. Water Resources Research 27, 1263–1269. https://doi.org/10.1029/91WR00367

Nordtvedt, J.-E., Kolltveit, K. (1991). Capillary pressure curves from centrifuge data by use of spline functions. SPE Reservoir Engineering, 6(04), 497–501. https://doi.org/10.2118/19019-pa

Rasoulzadeh, A., Bezaatpour, J., Azizi Mobaser, J., Fernández-Gálvez, J., 2025. Half-Century Review and Advances in Closed-Form Functions for Estimating Soil Water Retention Curves. Hydrology 12, 164. https://doi.org/10.3390/hydrology12070164

Šimůnek, J., Nimmo, J. R., 2005, Estimating soil hydraulic parameters from transient flow experiments in a centrifuge using parameter optimization technique. Water Resources Research, 41(4), 2004WR003379. https://doi.org/10.1029/2004WR003379

Tavangarrad, A.H., Hassanizadeh, S.M., Rosati, R., Digirolamo, L., Van Genuchten, M.T., 2019. Capillary pressure–saturation curves of thin hydrophilic fibrous layers: effects of overburden pressure, number of layers, and multiple imbibition–drainage cycles. Textile Research Journal 89, 4906–4915. https://doi.org/10.1177/0040517519844209

Turturro, A.C., Caputo, M.C., Gerke, H.H., 2022. Mercury intrusion porosimetry and centrifuge methods for extended-range retention curves of soil and porous rock samples. Vadose Zone Journal 21, e20176. https://doi.org/10.1002/vzj2.20176

van Genuchten, M. Th., 1980. A closed-form equation for predicting the hydraulic conductivity of unsaturated soils. Soil Science Society of America Journal, 44(5), 892–898. https://doi.org/10.2136/sssaj1980.03615995004400050002x

Wirgin, A., 2004. The inverse crime. https://doi.org/10.48550/ARXIV.MATH-PH/0401050

Received 21 October 2025
Accepted 4 February 2026